www.sciencemag.org/content/355/6320/78/suppl/DC1

Supplementary Material for

Rb1 and *Trp53* cooperate to suppress prostate cancer lineage plasticity, metastasis, and antiandrogen resistance

Sheng Yu Ku, Spencer Rosario, Yanqing Wang, Ping Mu, Mukund Seshadri, Zachary W. Goodrich, Maxwell M. Goodrich, David P. Labbé, Eduardo Cortes Gomez, Jianmin Wang, Henry W. Long, Bo Xu, Myles Brown, Massimo Loda, Charles L. Sawyers, Leigh Ellis,* David W. Goodrich*

*Corresponding author. Email: david.goodrich@roswellpark.org (D.W.G.); leigh.ellis@roswellpark.org (L.E.)

Published 6 January 2017, *Science* **355**, 78 (2017)
DOI: 10.1126/science.aah4199

This PDF file includes:

Materials and Methods

Mice

Construction and genotyping of all genetically engineered mouse alleles used has been described previously (*13, 20, 30*). Experimental mice were on a mixed C57BL/6:129/Sv:FVB genetic background. Mice were monitored daily, euthanized when moribund, and necropsied to verify diagnosis and collect tissue. Survival analysis by the Kaplan-Meier method was done with GraphPad Prism software. All animal work was performed under Roswell Park Cancer Institute IACUC approved protocols.

Histology, immunostaining, and microscopy

Prostate tissue is fixed in 10% neutral buffered formalin or phosphate-buffered 4% paraformaldehyde, paraffin embedded, and serially sectioned at 5-μm thickness. Sections are H&E stained for assessment of histopathology, and pathology verified by a pathologist (B.X.). Primary antibodies used for immunostaining are listed in Table S1. Immunostaining was developed using the ABC kit (Vector), followed by hematoxylin counterstaining. For senescence associated β-galactosidase staining, tissue specimens were embedded in OCT and cryosections prepared at 5-μm depth. Sections were fixed and stained as recommended using a senescence detection kit (Calbiochem). The Nuance multispectral imaging system (Perkin-Elmer) fitted to an Olympus SZX16 stereo microscope was used to image Brainbow 2.1 fluorescent proteins in whole mount, tumor bearing DKO prostate tissue.

Magnetic Resonance Imaging

Experimental MRI examinations were performed by the RPCI Translational Imaging shared resource in a 4.7T/33-cm horizontal bore magnet (GE NMR Instruments, Fremont, CA) equipped with AVANCE digital electronics (Bruker Biospec, Paravision 3.0.2; Bruker Medical Inc., Billerica, MA), a removable gradient coil insert (G060) generating a maximum field strength of 950 mT/m and a custom-designed 35-mm RF transmit-receive coil. Preliminary localizer images were acquired for subsequent slice prescription. Multislice axial T2-weighted (T2W) spin echo RARE sequence images were acquired using the following parameters: Field of view (FOV) = 3.20 x 3.20 cm, matrix (MTX) = 256 x 192, slice thickness = 1 mm, NEX = 4, TR = 2500 ms, TE_{eff} = 41.0 ms, RARE/Echoes= 8/8. The number of slices varied depending on the size of the animal. Following image acquisition, raw image sets were transferred to a processing workstation and converted into Analyze™ format (AnalyzeDirect, version 7.0; Overland Park, KS). All post processing of imaging data was carried out in Analyze™ and MATLAB. Volumetric calculations were obtained by tracing a region of interest (ROI) around the prostate (all affected lobes) excluding areas of cystic dilations.

RNA-sequencing analysis

RNA-sequencing (RNA-seq) was performed by the RPCI Genomics shared resource. Sequencing libraries were prepared with the TruSeq Stranded Total RNA kit (Illumina Inc), from 1 μg total RNA following manufacturer's instructions. After ribosomal RNA depletion, RNA is purified, fragmented and primed for cDNA synthesis. Fragmented RNA is reverse transcribed into first strand cDNA using random

primers. AMPure XP beads are used to separate the ds cDNA from the second strand reaction mix resulting in blunt-ended cDNA. A single 'A' nucleotide is then added to the 3' ends of the blunt fragments. Multiple indexing adapters, containing a single 'T' nucleotide on the 3' end of the adapter, are ligated to the ends of the ds cDNA, preparing them for hybridization onto a flow cell. Libraries are purified and validated for appropriate size on a 2100 Bioanalyzer High Sensitivity DNA chip (Agilent Technologies, Inc.). The DNA library is quantitated using KAPA Biosystems qPCR kit, and normalized to 2nM prior to pooling. Libraries are pooled in an equimolar fashion and diluted to 10pM. Library pools are clustered and run on a HiSeq2500 rapid mode sequencer according to the manufacturer's recommended protocol (Illumina Inc.).

Raw reads passing the Illumina RTA quality filter are pre-processed using FASTQC for sequencing base quality control. Reads are mapped to the mouse reference genome (mm9) and RefSeq annotation database using Tophat. A second round of quality control using RSeQC is applied to mapped bam files to identify potential RNA-seq library preparation problems. The number of reads aligning to each gene is calculated using HTSeq and for each gene the corresponding RPKM value is calculated.

GATK best practices for variant calling with RNA-seq data were used to analyze the *Trp53* gene (https://www.broadinstitute.org/gatk/guide/article?id=3891). Variants were filtered by a minimum allele frequency of 5% and further annotated using ANNOVAR. Only variants with amino acid changes are considered and corresponding human mutations are determined by aligning the mutant mouse protein sequence with the human TP53 protein sequence.

For differential gene expression analysis, RNA-seq counts were processed to remove genes lacking expression in more than 80% of samples. Scale normalization was done using the Limma package in R. After Voom transformation, data from primary SKO, DKO, and TKO tumors were then compared to generate differentially expressed gene lists with $P<0.05$ and $logFC>1.5$. Genes differentially expressed between SKO and DKO tumors were then applied across all samples to generate a scaled heatmap, constructed using the "Gplots" and "Heatmap.2" packages in R. Euclidian distances and hierarchal clustering were utilized to determine sample similarity. Principal Component Analysis was conducted utilizing the "PrComp" package in R.

A weighted rank list of the differentially expressed genes was constructed by taking the log2 of the p-value of all genes multiplied by the sign of the fold change. Using the pre-ranked list, Gene Set Enrichment Analysis (GSEA) was performed using the GSEAPreranked tool (**http://www.broadinstitute.org/-gsea**) to ascertain relationships with existing gene expression profiles (Hallmarks, Curated, and Oncogenic Signatures) in the Molecular Signature Database (MSigDB).

A 50 gene weighted rank list distinguishing human PADC and NEPC was obtained from Beltran et al. (*23*), 35 of which had orthologues in the mouse and were expressed in our tissue samples. These 35 genes were used to assign a score to each sample by log-transforming raw RNA-sequencing counts, multiplying by the established weighting, and adding all values for each gene in the signature. Data for these 35 genes was obtained from Beltran NEPC and PADC samples from cBioPortal as log-transformed values and were used to calculate scores as above. Values were then plotted according to human designation (NEPC, PADC) and mouse genotype (SKO, DKO, TKO).

ChIP-sequencing analysis

Fresh-frozen prostatic tumor tissue was pulverized (Cryoprep Pulvrizer, Covaris), resuspended in PBS + 1% formaldehyde, and incubated at room temperature for 20 minutes. Fixation was stopped by addition of 0.125 M glycine (final concentration) for 15 minutes at room temperature, then washing in ice cold PBS + EDTA-free protease inhibitor cocktail (PIC; #04693132001, Roche). Chromatin was isolated from biological triplicates by the addition of lysis buffer (0.1% SDS, 1% Triton X-100, 10 mM Tris-HCl (pH 7.4), 1 mM EDTA (pH 8.0), 0.1% NaDOC, 0.13 M NaCl, 1X PIC) + sonication buffer (0.25% sarkosyl, 1 mM DTT) to the samples, which were maintained on ice for 30 minutes. Lysates were sonicated (E210 Focused-ultrasonicator, Covaris) and the DNA was sheared to an average length of ~200-500 bp. Genomic DNA (input) was isolated by treating sheared chromatin samples with RNase (30 minutes at 37°C), proteinase K (30 minutes at 55°C), de-crosslinking buffer (1% SDS, 100 mM NaHCO3 (final concentration), 6-16 hours at 65°C), followed by purification (#28008, Qiagen). DNA was quantified on a NanoDrop spectrophotometer, using the Quant-iT High-Sensitivity dsDNA Assay Kit (#Q33120, Thermo Fisher Scientific). On ice, H3K27me3 (5 µl, #07-449, Millipore) or H3K4me3 (5 µl, #17-614, Millipore) antibodies were conjugated to a mix of washed Dynalbeads protein A and G (Thermo Fisher Scientific), and incubated on a rotator (overnight at 4°C) with 1.3 µg of chromatin. ChIP'ed complexes were washed, sequentially treated with RNase (30 minutes at 37°C), proteinase K (30 minutes at 55°C), de-crosslinking buffer (1% SDS, 100 mM NaHCO3 (final concentration), 6-16 hours at 65°C), and purified (#28008, Qiagen). The concentration and size distribution of the immunoprecipitated DNA was measured using the Bioanalyzer High Sensitivity DNA kit (#5067-4626, Agilent). Dana-Farber Cancer Institute Molecular Biology Core Facilities prepared libraries from 2 ng of DNA, using the ThruPLEX DNA-seq kit (#R400427, Rubicon Genomics), according to the manufacturer's protocol; finished libraries were quantified by the Qubit dsDNA High-Sensitivity Assay Kit (#32854, Thermo Fisher Scientific), by an Agilent TapeStation 2200 system using D1000 ScreenTape (# 5067-5582, Agilent), and by RT-qPCR using the KAPA library quantification kit (# KK4835, Kapa Biosystems), according to the manufacturers' protocols; ChIP-seq libraries were uniquely indexed in equimolar ratios, and sequenced to a target depth of 40M reads on an Illumina NextSeq500 run, with single-end 75bp reads. BWA (version 0.6.1) was used to align the ChIP-seq datasets to build version NCB37/MM9 of the mouse genome. Alignments were performed using default parameters that preserved reads mapping uniquely to the genome without mismatches. Bam files were concatenated to sum the biological replicates of each state and bigwiggle files were calculated for comparing the different states.

Cell culture and growth assays

SKO, DKO and TKO prostate cancer cell lines were isolated from respective GEMMs, and cultured in PrE media described previously (*30*). LNCaP-AR NS, shRB, and shRBP53 cells were cultured in RPMI1640 with 10% FBS, 2mM L-glutamine, 10mM HEPES (10mM), and 1% P/S (Corning). Enzalutamide, GSK126, and EPZ6438 were purchased from Xcessbio. Enzalutamide was used at 10 µM and Ezh2i as indicated. R1881 and dihydrotestosterone (DHT) was used at 1nM.

For cell growth assays, 10,000 cells were plated in a 24-well plate and cell treated as indicated the next day. Mouse lines were treated for 3 days without drug replenishment while human lines were treated for 6 days, refreshing drug on day 3. Trypan blue excluding cells were counted with a hemocytometer then normalized to DMSO control to determine relative cell growth. For colony forming assays, 500 cells were plated into each well of a 6 well plate and cells treated as indicated the following day. Cells were cultured for 7-10 days without drug replenishment, then fixed and stained with crystal violet. Colony formation was measured using the Colony Area plugin for ImageJ. For scratch assays, a confluent monolayer of cells pre-treated with or without Ezh2i (2.5 μM) as indicated was scratched and then imaged by phase contrast microscopy at the indicated times.

Transplantation drug sensitivity assay

Approximately 8 mm3 pieces of a DKOCr tumor was implanted subcutaneously into castrated male SCID mice. When tumors reached 100 mm3, mice were randomized into four groups for daily treatment: (1) Vehicle (1% carboxymethyl cellulose, 0.1% Tween-80, 5% DMSO by oral gavage+20% Captisol solution by IP), (2) Enzalutamide 30mg/kg/daily by oral gavage, (3) GSK503 150mg/kg/daily by IP, (4) combination. Mice were weighed and tumors measured every other day. Mouse weights did not change significantly over the course of the experiment, demonstrating minimal toxicity. Tumor size was calculated using the formula length x width2 x 0.5.

Real-time RT-PCR and western blotting

RNA was extracted using TRIzol (ThermoFisher Scientific) following the manufacture's protocol, and then subjected to cDNA synthesis using iScript kit (Bio-rad). Real-time PCR was performed using the iTag universal SYBR Green kit (Bio-rad) and subsequently analyzed in a CFX Connect system (Bio-rad). The sequences of primers used have been listed in Table S2.

Cell lysates for western blotting were prepared using RIPA buffer (Sigma) containing a protease and phosphatase inhibitor cocktail (Roche). 50 μg total protein was subjected to SDS-PAGE electrophoresis, then transferred to a nitrocellulose membrane. The membrane was blocked in 5% non-fat milk for one hour at room temperature, followed by primary antibody incubation. Antibodies used have been listed in Table S1. and αGAPDH (1:5000, Cell Signaling). The immunostaining was visualized using a chemiluminescent substrate kit (ThermoFisher Scientific).

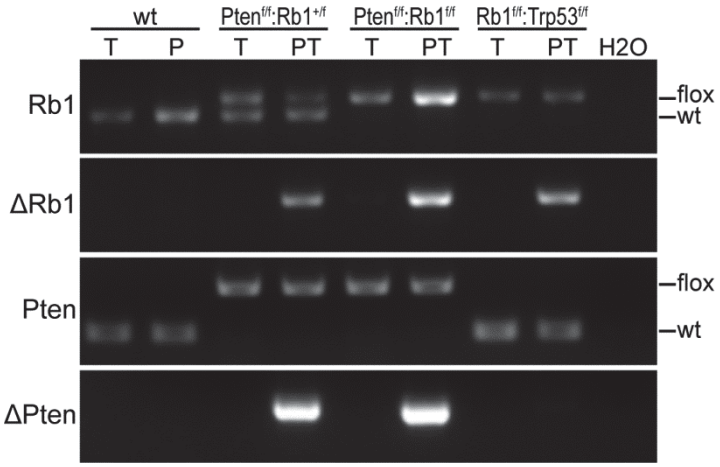

Fig. S1. Prostate specific Cre mediated recombination.

Genomic DNA extracted from tail (T), prostate (P), or prostate tumor (PT) tissue of the indicated genotypes was amplified by PCR to detect wild type (wt), floxed (flox) or Cre recombined alleles (Δ) of the Rb1 and Pten genes. PCR bands were resolved by agarose gene electrophoresis and stained with ethidium bromide.

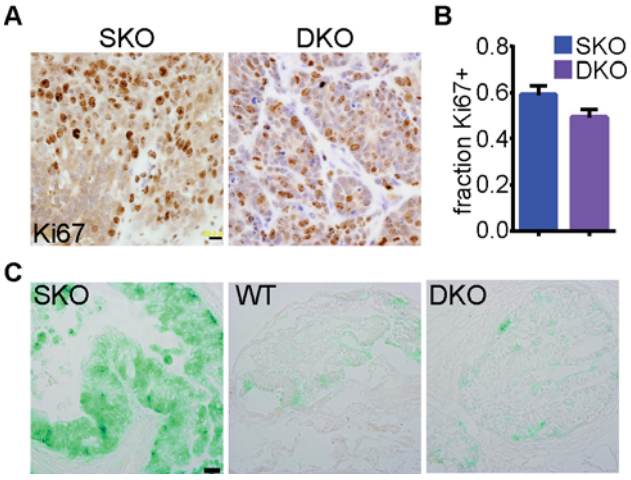

Fig. S2. *Rb1* loss has little effect on end stage tumor cell proliferation, but abrogates cellular senescence in Pten deficient premalignant prostate epithelium.

(A) Tumor tissue sections from mice of the indicated genotypes were stained with Ki67 antibody, and a representative image is shown. (B) The fraction of Ki67+ tumor cells was counted manually. The graph shows the mean and standard error for 3 (SKO) or 4 (DKO) tumors. (C) Frozen prostate tissue sections from 12-13 week old mice of the indicated genotype were stained for senescence associated beta-galactosidase activity. Representative brightfield images are shown. Magnification bars represent 100 microns.

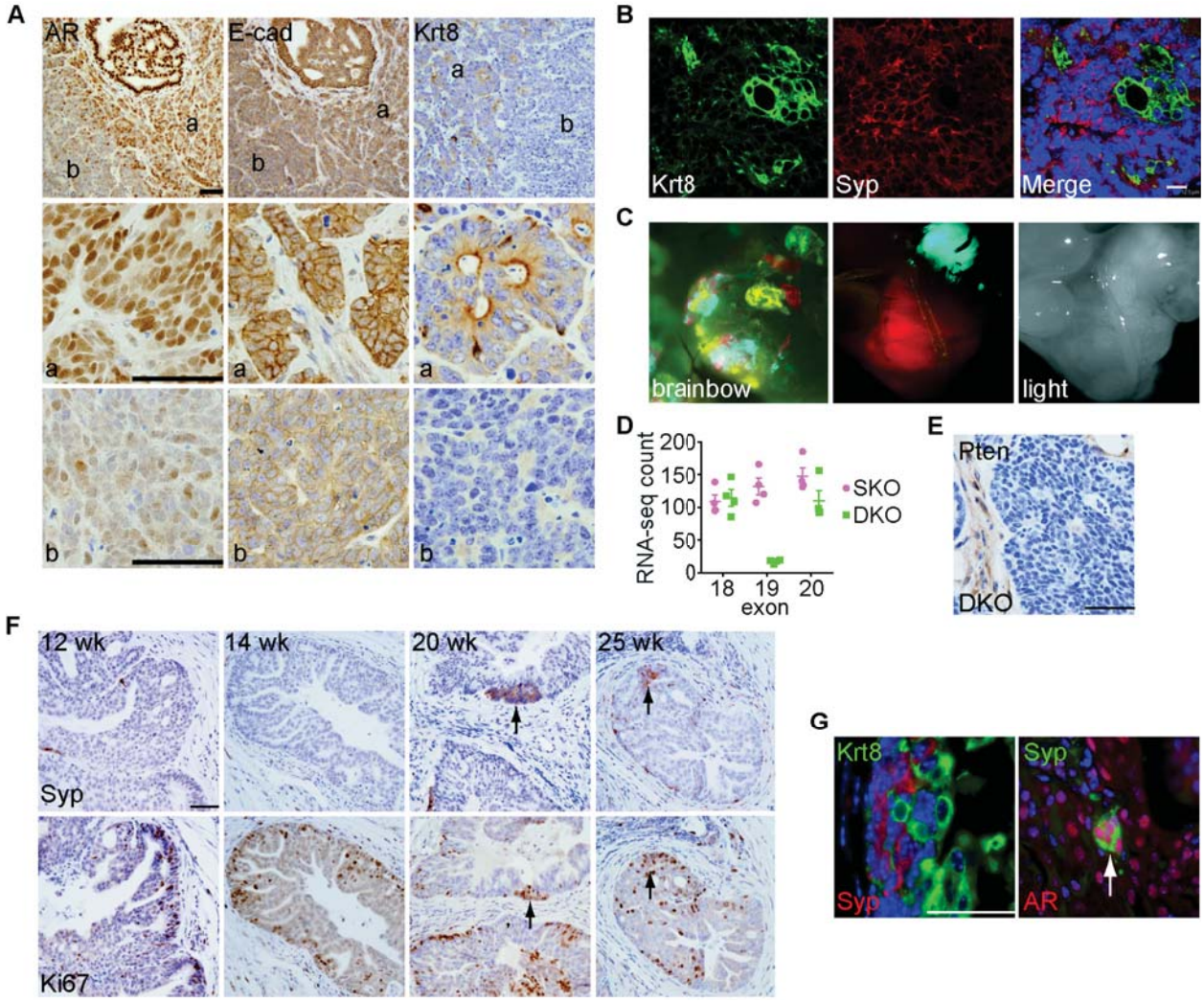

Fig. S3. DKO prostate tumors exhibit lineage plasticity.
(A) Tissue sections from a contiguous, end stage DKO tumor were immunostained for the indicated proteins and representative microscopic images shown. Regions "a" and "b" represent regions of distinct molecular phenotype and are magnified in the lower panels. Magnification bars are100 microns. (B) A DKO tumor section was stained for both Krt8 and Syp, and DNA counterstained with DAPI. The section was imaged under confocal fluorescence microscopy. The merged image demonstrates lack of overlap between Krt8 and Syp immunostaining. Magnification bar is 12.5 microns. (C) Whole mount prostate tissue from a 36 week old DKO mouse containing the Brainbow 2.1 allele was imaged by multispectral or light microscopy. The left panel shows areas of clonal expansion with each clone marked with one of the four possible Brainbow fluorescent proteins. The center and right panels shows tissue from one mouse containing two clonally distinct primary tumors (red, blue). All primary tumors examined to date (*N*=7) are monocolor. (D) RNA-seq read counts mapping to the indicated *Rb1* exons are shown for tumors of the indicated genotypes. Bars represent the mean and standard error. Very few reads map to exon 19, the exon deleted by Cre in DKO tumors, demonstrating near complete gene deletion. (E) Tumor tissue sections from a DKO mouse immunostained for Pten are shown. DKO tumors were uniformly Pten negative. Magnification bar is 100 micron. (F) Prostate tissue sections from DKO mice of the indicated ages were immunostained for

Syp or Ki67. Arrows show foci of cells staining positive for both Ki67 and Syp. Prior to 20 weeks, Ki67 positive neoplasia was Syp negative. Magnification bars are 100 microns. (G) Prostate tissue sections from a 25 week old DKO mouse immunostained for the indicated proteins is shown. The left panel shows the earliest Syp^{high} cells detected within PIN lesions are $Krt8^{low}$. Arrows in the right panel shows the earliest Syp^{high} cells detected in DKO PIN lesions are AR^{high}. Magnification bar is 100 microns

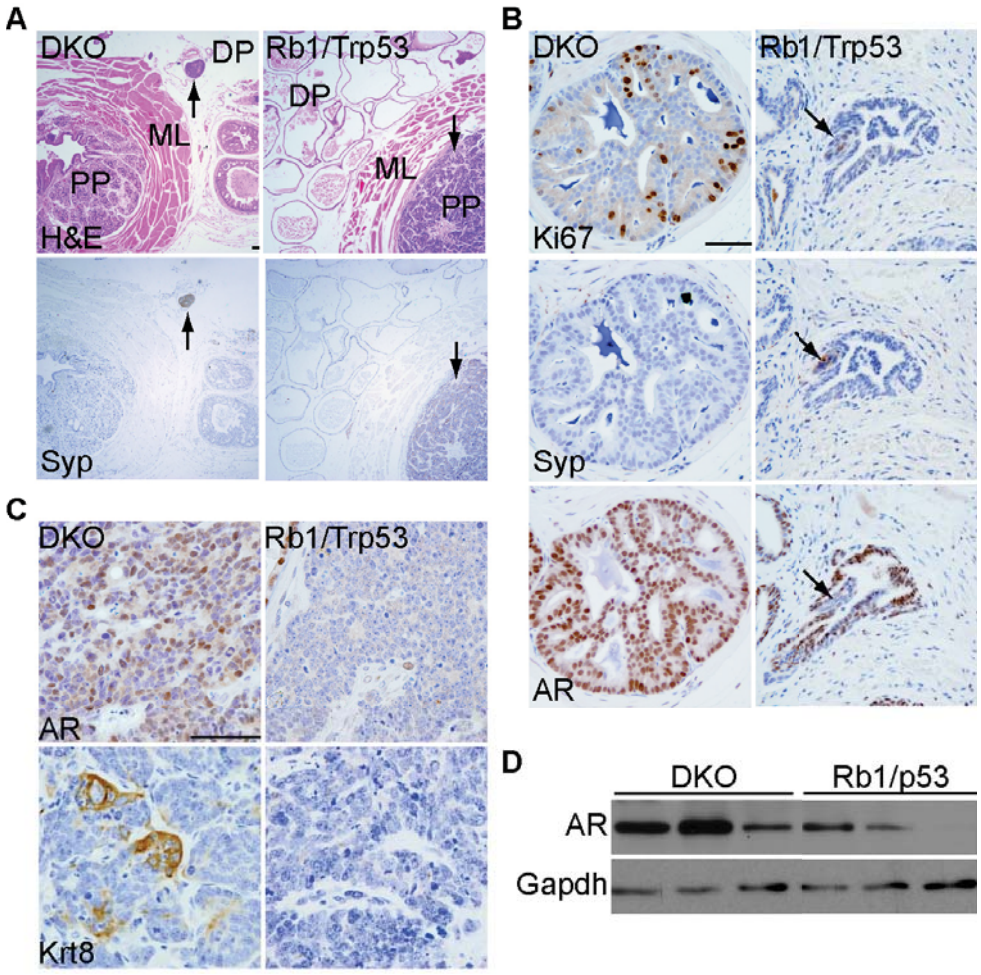

Fig. S4. DKO and PBCre4:*Rb1*$^{f/f}$:*Trp53*$^{f/f}$ prostate cancers have distinct phenotypes. (A) Tissue sections from DKO or PBCre4:*Rb1*$^{f/f}$:*Trp53*$^{f/f}$ (Rb1/Trp53) mice are stained with H&E or immuostained for Syp. Images show the proximal (PP) and distal (DP) regions of the prostate as well as the muscular layer (ML) separating the two. Arrows highlight Syp positive tumors arising from different anatomical locations in these mice. Magnification bar is 100 microns. (B) Tissue sections from the indicated mice were stained for Ki67, Syp, or AR. The images show Ki67 positive early PIN lesions within the proximal region of the prostate. Early proximal PIN lesions from DKO mice are Syp^{low}:AR^{high}. Very early proximal PIN lesions from PBCre4:*Rb1*$^{f/f}$:*Trp53*$^{f/f}$ mice are Syp^{high}:AR^{low}. Magnification bar is 100 microns. (C) Tumor tissue sections from end stage tumors of the indicated genotypes immunostained for AR or Krt8 to highlight differences in expression. Magnification bar is 100 microns. (D) Three primary tumor specimens from each of the indicated genotypes were extracted and protein analyzed for AR expression by western blotting. Gapdh serves as the protein loading control.

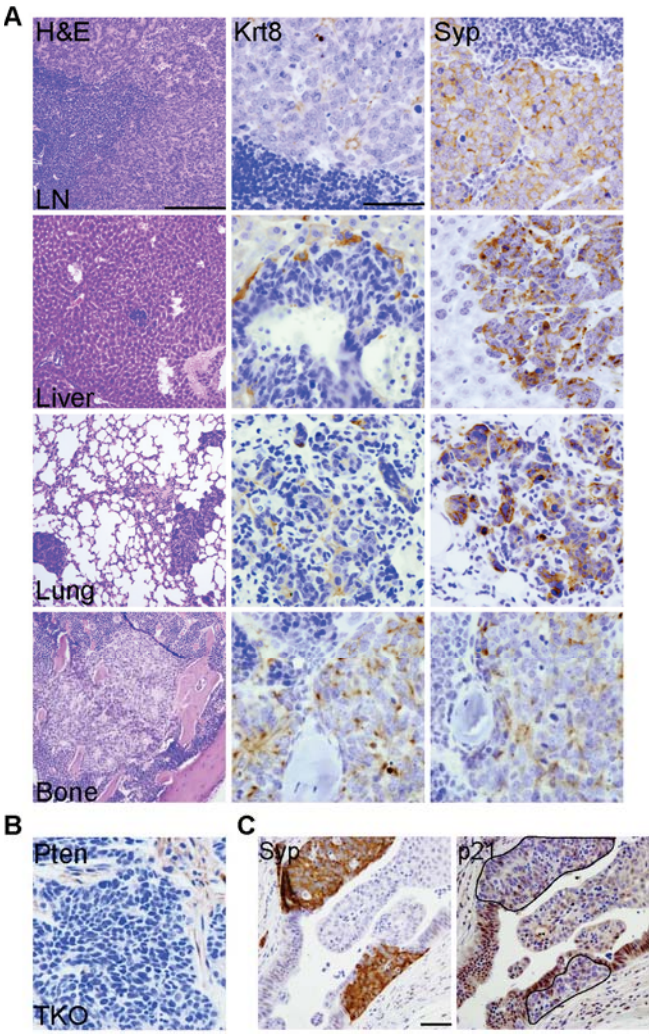

Fig. S5. Trp53 loss alters prostate cancer phenotype.

(A) Metastatic tumor sections from the indicated tissues (lymph node=LN) of TKO mice were stained for H&E, Krt8, or Syp. Magnification bar is 100 microns. (B) Primary tumor section from a TKO mouse was immunostained for Pten and a representative image shown. TKO tumors lack cells with detectable Pten, but Pten is readily detectable in surrounding stromal cells. Lack of pAKT in these tumors is not explained by incomplete Pten deletion. (C) Prostate tissue sections from a 14 week old PBCre4:$Rb1^{f/f}$:$Trp53^{f/+}$ mouse retaining one wild type Trp53 allele were immunostained for Syp or p21. Foci of Syp^{high} cells appear earlier than in DKO mice. Black lines outline areas of reduced p21 expression coincident with Syp expression. Magnification bar is 100 microns.

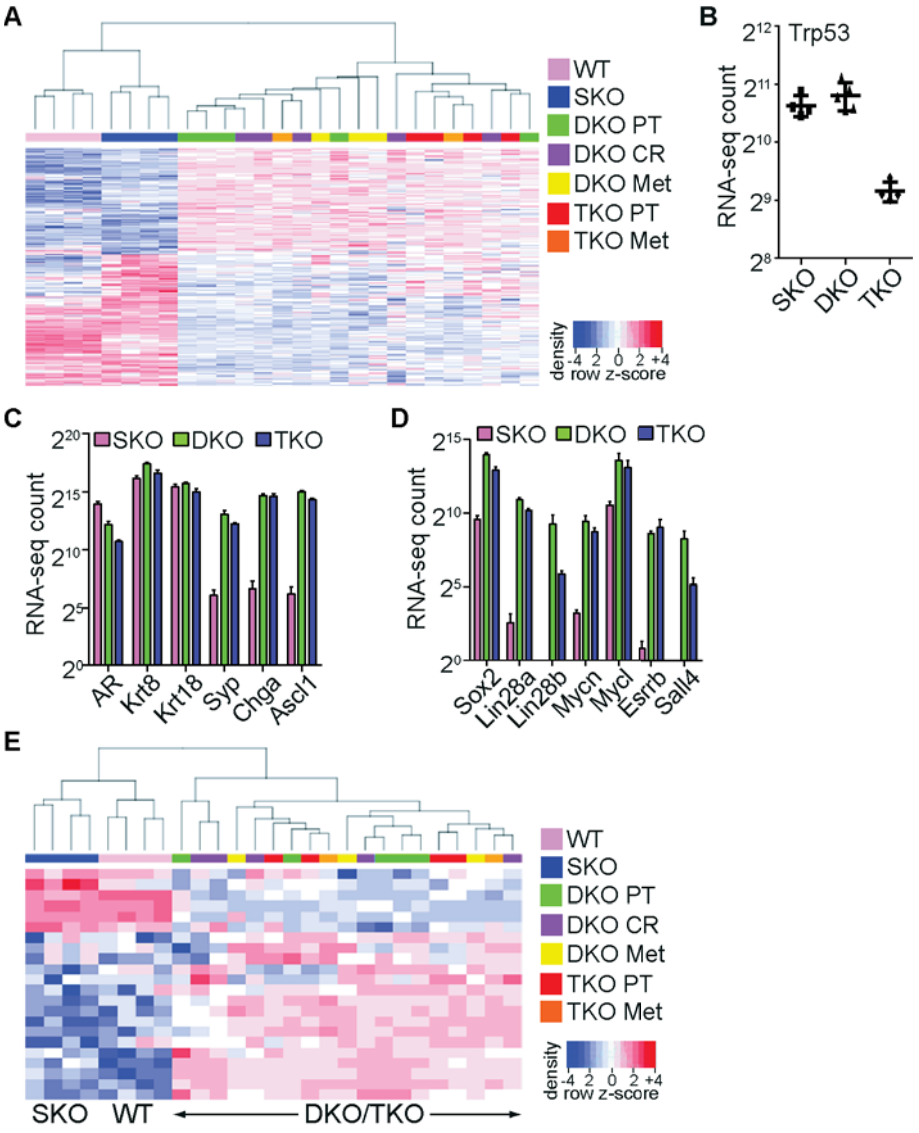

Fig. S6. *Rb1* loss in prostate cancer results in widespread changes in gene expression.

(A) A heat map shows hierarchical clustering of RNA-seq data from wild type prostate tissue (WT) as well as primary (PT), metastatic (Met), or castrate recurrent (Cr) prostate tumors of the indicated genotypes. Gene expression patterns cluster by genotype. (B) RNA-seq counts mapping to the Trp53 locus are shown from tumor specimens of the indicated genotypes. DKO tumors do not exhibit spontaneous silencing of *Trp53* expression. (C) Normalized RNA-seq counts are shown for select luminal epithelial and neuroendocrine marker genes demonstrating changes consistent with neuroendocrine lineage transformation. (D) Normalized RNA-seq counts are shown for stem cell reprogramming factors indicating up regulation in *Rb1* deficient tumors. (E) The Beltran human NEPC signature was used to cluster gene expression patterns in SKO, DKO, and TKO tumors. As in humans, the signature accurately distinguishes *Rb1* proficient SKO PADC from *Rb1* deficient DKO and TKO NEPC-like tumors.

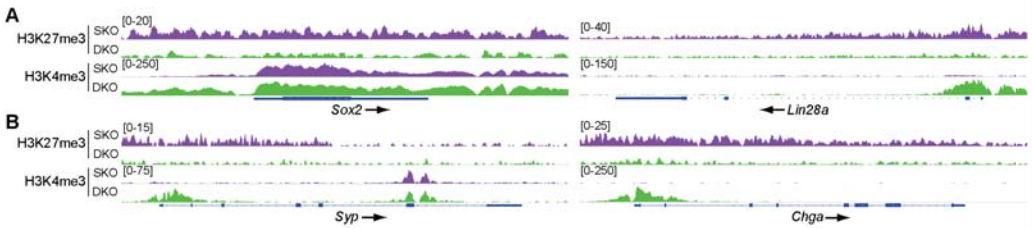

Fig. S7. Rb1 loss in prostate cancer causes changes in histone post-translational modifications.
(A) ChIP-seq analysis was performed for the indicated histone H3 methylation modifications on SKO and DKO tumors (N=3 per genotype). The figure shows the sum of the read counts mapping to the vicinity of two stem cell reprogramming factor genes. Arrows indicate the direction of transcription. Overall, SKO tumors exhibit greater H3K27me3 modification and DKO tumors exhibit greater H3K4me3, consistent with the gene expression changes observed. (B) Data generated in (A) was analyzed for read counts mapping to two neuroendocrine lineage marker genes.

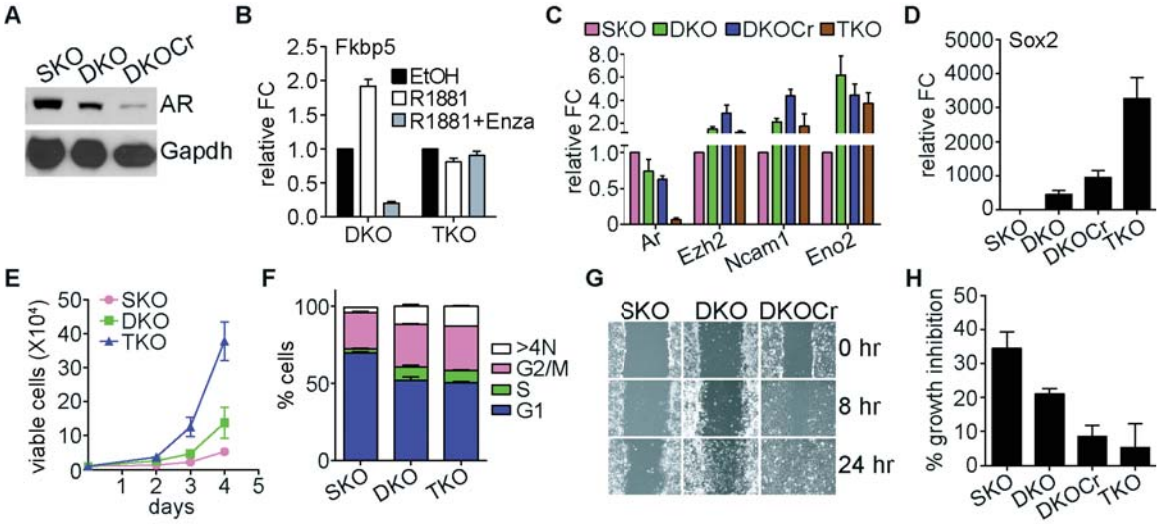

Fig. S8. Prostate cancer cell lines mirror tumor phenotypes.

(A) Protein was extracted from the indicated cell lines and analyzed for AR by western blotting. Gapdh serves as the protein loading control. (B) RNA was extracted from the indicated cell lines treated with the AR ligand R1881 or enzalutamide (Enza) and analyzed for the AR target gene *Fkbp5* by real time RT-PCR. The graph shows the mean and standard error from 2-3 experiments. (C) RNA was extracted from the indicated cell lines and RNA expressed from the listed genes measured by real time RT-PCR. The mean and standard error of fold change (FC) relative to the SKO cell line for 3 experiments is shown. (D) RNA was analyzed for *Sox2* expression as in (C). Results are from 4 experiments. (E) Cell accumulation over time was measured for the indicated cell lines. The data represent the mean and standard deviation of 3 experiments. (F) The cell cycle distribution of the asynchronously growing cell lines listed was measured by propidium iodide staining and flow cytometry. The data represent the mean and standard error of 3 experiments. (G) Scratch assays were performed on the indicated cell lines and representative images at the indicated times is shown. (H) The indicated cell lines were treated with enzalutamide and extent of growth inhibition shown. The results show the mean and standard error for 3 experiments.

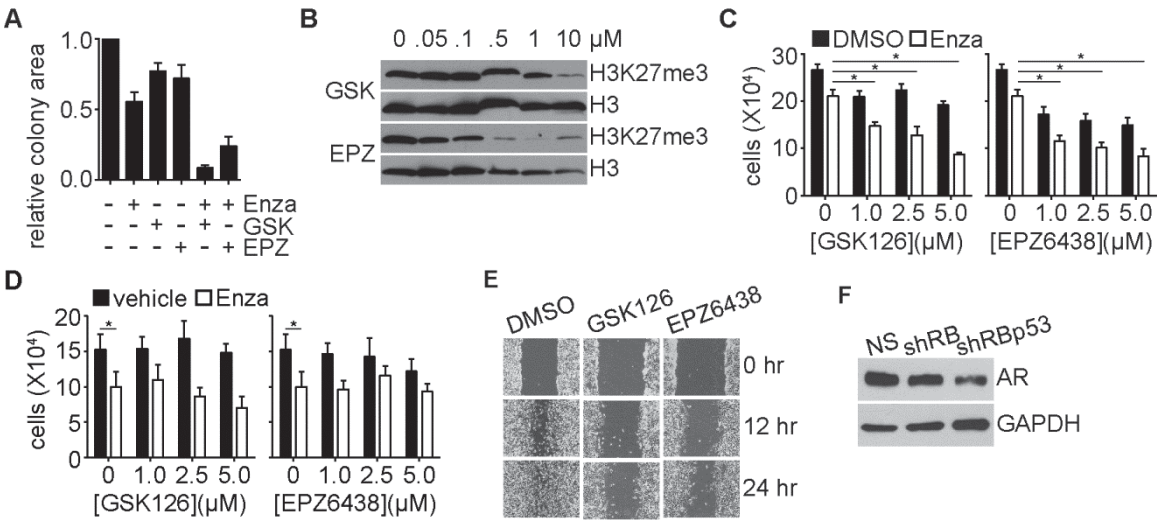

Fig. S9. Ezh2 inhibition alters prostate cancer cell phenotype.

(A) Colony formation assays were performed as in Fig. 4B and colony area quantitated by image analysis. The graph shows the mean and standard error of 5 experiments normalized to vehicle control. (B) DKOCr cells were treated with indicated concentrations of Ezh2i (GSK=GSK126, EPZ=EPZ6438), protein was extracted, and protein analyzed for histone H3K27 trimethylation (H3K27me3) or total H3. (C) A DKO cell line was treated with Ezh2i and/or enzalutamide (Enza) and effects on cell growth measured as in figure 4A. Asterisks mark significant differences ($P<0.05$). (D) A SKO cell line was treated and analyzed as in (C). (E) A DKO cell line was pre-treated with Ezh2i or vehicle, and scratch assays subsequently performed. A representative result shows decreased motility of cells pre-treated with Ezh2i. (F) LNCaP-AR cell line derivatives expressing a non-silencing shRNA (NS), RB1 shRNA (shRB), or RB1/TP53 shRNA (shRBp53) were extracted and total protein analyzed for AR levels by western blotting. Gapdh serves as protein loading control.

Table S1: Antibodies used

Antibody	Host	Dilution	Source
AR (N-20)	Rabbit	1:400 (IHC)* 1:2000 (western) 1:100 (IF)†	Santa Cruz
P21 (H-164)	Rabbit	1:200	Santa Cruz
P63 (4A4)	Mouse	1:200	Santa Cruz
CK8 (THOMA-I)	Rat	1:400 (IHC) 1:10 (IF)	Research diagnostics
Synaptophysin (18-0130)	Rabbit	1:600 (IHC) 1:100 (IF) 1:500 (western)	Invitrogen
Synaptophysin (SY38.ab8049)	Mouse	1:50 (IF)	Abcam
Phospho-Akt (Ser473)	Rabbit	1:100	Cell Signaling
Pten	Rabbit	1:400	Cell Signaling
E-Cad	Mouse	1:100	BD Biosciences
Ezh2	Rabbit	1:400	Cell Signaling
Sox2	Rabbit	1:200	Cell Signaling
H3K27me3	Rabbit	1:1000 (western) 1:1200 (IHC)	Cell Signaling
H3	Rabbit	1:2000	Cell Signaling
Gapdh	Rabbit	1:5000	Cell Signaling
Ki67	Rabbit	1:1000	Novocastra
Anti-Mouse IgG	Goat	1:1000	Invitrogen

Alexa Fluor 488			
Anti-Rat IgG Alexa Fluor 488	Goat	1000	Invitrogen
Anti-Rabbit IgG Alexa Fluor 594	Goat	1000	Invitrogen

*Immunohistochemistry
†Immunofluorescence

Table S2: Primers used for real time RT-PCR

Primer	Sequence
AR-forward	CGACTATTACTTTCCACCCCAG
AR-reverse	TGCTGGCACATAGATACTTCTG
Krt8-forward	TGTTGAGCCCCTTGAAGC
Krt8-reverse	GGTCTCCAGCATCTTGTTCTG
Fkbp5-forward	GACACCAAAGAAAAGCTGACG
Fkbp5-reverse	CTTCTCTGACAGGCCGTATTC
Ezh2-forward	TCCCGTTAAAGACCCTGAATG
Ezh2-reverse	TGAAAGTGCCATCCTGATCC
Eno2-forward	TCAAGGACAAGTATGGCAAGG
Eno2-reverse	ACCGATCACCATCTTTTCCG
Ncam1-forward	CCCCACAGGAGTTTAAGGAAG
Ncam1-reverse	GTTGGACAGGACTATGAACCG
Sox2-forward	CACATGGCCCAGCACTAC
Sox2-reverse	CCCTCCCAATTCCCTTGTATC
L32-forward	TTCCTGGTCCACAACGTCAAG
L32-reverse	TGTGAGCGATCTCGGCAC

References and Notes

1. L. V. Sequist, B. A. Waltman, D. Dias-Santagata, S. Digumarthy, A. B. Turke, P. Fidias, K. Bergethon, A. T. Shaw, S. Gettinger, A. K. Cosper, S. Akhavanfard, R. S. Heist, J. Temel, J. G. Christensen, J. C. Wain, T. J. Lynch, K. Vernovsky, E. J. Mark, M. Lanuti, A. J. Iafrate, M. Mino-Kenudson, J. A. Engelman, Genotypic and histological evolution of lung cancers acquiring resistance to EGFR inhibitors. *Sci. Transl. Med.* **3**, 75ra26 (2011). doi:10.1126/scitranslmed.3002003 Medline

2. M. J. Niederst, L. V. Sequist, J. T. Poirier, C. H. Mermel, E. L. Lockerman, A. R. Garcia, R. Katayama, C. Costa, K. N. Ross, T. Moran, E. Howe, L. E. Fulton, H. E. Mulvey, L. A. Bernardo, F. Mohamoud, N. Miyoshi, P. A. VanderLaan, D. B. Costa, P. A. Jänne, D. R. Borger, S. Ramaswamy, T. Shioda, A. J. Iafrate, G. Getz, C. M. Rudin, M. Mino-Kenudson, J. A. Engelman, RB loss in resistant EGFR mutant lung adenocarcinomas that transform to small-cell lung cancer. *Nat. Commun.* **6**, 6377 (2015). doi:10.1038/ncomms7377 Medline

3. H. Beltran, S. Tomlins, A. Aparicio, V. Arora, D. Rickman, G. Ayala, J. Huang, L. True, M. E. Gleave, H. Soule, C. Logothetis, M. A. Rubin, Aggressive variants of castration-resistant prostate cancer. *Clin. Cancer Res.* **20**, 2846–2850 (2014). doi:10.1158/1078-0432.CCR-13-3309 Medline

4. C. J. Pezaro, A. Omlin, D. Lorente, D. Nava Rodrigues, R. Ferraldeschi, D. Bianchini, D. Mukherji, R. Riisnaes, A. Altavilla, M. Crespo, N. Tunariu, J. S. de Bono, G. Attard, Visceral disease in castration-resistant prostate cancer. *Eur. Urol.* **65**, 270–273 (2014). doi:10.1016/j.eururo.2013.10.055 Medline

5. H. Beltran, D. Prandi, J. M. Mosquera, M. Benelli, L. Puca, J. Cyrta, C. Marotz, E. Giannopoulou, B. V. S. K. Chakravarthi, S. Varambally, S. A. Tomlins, D. M. Nanus, S. T. Tagawa, E. M. Van Allen, O. Elemento, A. Sboner, L. A. Garraway, M. A. Rubin, F. Demichelis, Divergent clonal evolution of castration-resistant neuroendocrine prostate cancer. *Nat. Med.* **22**, 298–305 (2016). doi:10.1038/nm.4045 Medline

6. C. C. Guo, J. Y. Dancer, Y. Wang, A. Aparicio, N. M. Navone, P. Troncoso, B. A. Czerniak, TMPRSS2-ERG gene fusion in small cell carcinoma of the prostate. *Hum. Pathol.* **42**, 11–17 (2011). doi:10.1016/j.humpath.2010.05.026 Medline

7. T. L. Lotan, N. S. Gupta, W. Wang, A. Toubaji, M. C. Haffner, A. Chaux, J. L. Hicks, A. K. Meeker, C. J. Bieberich, A. M. De Marzo, J. I. Epstein, G. J. Netto, ERG gene rearrangements are common in prostatic small cell carcinomas. *Mod. Pathol.* **24**, 820–828 (2011). doi:10.1038/modpathol.2011.7 Medline

8. S. R. Williamson, S. Zhang, J. L. Yao, J. Huang, A. Lopez-Beltran, S. Shen, A. O. Osunkoya, G. T. MacLennan, R. Montironi, L. Cheng, ERG-TMPRSS2 rearrangement is shared by concurrent prostatic adenocarcinoma and prostatic small cell carcinoma and absent in small cell carcinoma of the urinary bladder: Evidence supporting monoclonal origin. *Mod. Pathol.* **24**, 1120–1127 (2011). doi:10.1038/modpathol.2011.56 Medline

9. A. M. Aparicio, L. Shen, E. L. N. Tapia, J.-F. Lu, H.-C. Chen, J. Zhang, G. Wu, X. Wang, P. Troncoso, P. Corn, T. C. Thompson, B. Broom, K. Baggerly, S. N. Maity, C. J. Logothetis, Combined tumor suppressor defects characterize clinically defined aggressive

variant prostate cancers. *Clin. Cancer Res.* **22**, 1520–1530 (2016). doi:10.1158/1078-0432.CCR-15-1259 Medline

10. H. L. Tan, A. Sood, H. A. Rahimi, W. Wang, N. Gupta, J. Hicks, S. Mosier, C. D. Gocke, J. I. Epstein, G. J. Netto, W. Liu, W. B. Isaacs, A. M. De Marzo, T. L. Lotan, Rb loss is characteristic of prostatic small cell neuroendocrine carcinoma. *Clin. Cancer Res.* **20**, 890–903 (2014). doi:10.1158/1078-0432.CCR-13-1982 Medline

11. D. Robinson, E. M. Van Allen, Y.-M. Wu, N. Schultz, R. J. Lonigro, J.-M. Mosquera, B. Montgomery, M.-E. Taplin, C. C. Pritchard, G. Attard, H. Beltran, W. Abida, R. K. Bradley, J. Vinson, X. Cao, P. Vats, L. P. Kunju, M. Hussain, F. Y. Feng, S. A. Tomlins, K. A. Cooney, D. C. Smith, C. Brennan, J. Siddiqui, R. Mehra, Y. Chen, D. E. Rathkopf, M. J. Morris, S. B. Solomon, J. C. Durack, V. E. Reuter, A. Gopalan, J. Gao, M. Loda, R. T. Lis, M. Bowden, S. P. Balk, G. Gaviola, C. Sougnez, M. Gupta, E. Y. Yu, E. A. Mostaghel, H. H. Cheng, H. Mulcahy, L. D. True, S. R. Plymate, H. Dvinge, R. Ferraldeschi, P. Flohr, S. Miranda, Z. Zafeiriou, N. Tunariu, J. Mateo, R. Perez-Lopez, F. Demichelis, B. D. Robinson, M. Schiffman, D. M. Nanus, S. T. Tagawa, A. Sigaras, K. W. Eng, O. Elemento, A. Sboner, E. I. Heath, H. I. Scher, K. J. Pienta, P. Kantoff, J. S. de Bono, M. A. Rubin, P. S. Nelson, L. A. Garraway, C. L. Sawyers, A. M. Chinnaiyan, Integrative clinical genomics of advanced prostate cancer. *Cell* **161**, 1215–1228 (2015). doi:10.1016/j.cell.2015.05.001 Medline

12. Cancer Genome Atlas Research Network, The molecular taxonomy of primary prostate cancer. *Cell* **163**, 1011–1025 (2015). doi:10.1016/j.cell.2015.10.025 Medline

13. S. Wang, J. Gao, Q. Lei, N. Rozengurt, C. Pritchard, J. Jiao, G. V. Thomas, G. Li, P. Roy-Burman, P. S. Nelson, X. Liu, H. Wu, Prostate-specific deletion of the murine Pten tumor suppressor gene leads to metastatic prostate cancer. *Cancer Cell* **4**, 209–221 (2003). doi:10.1016/S1535-6108(03)00215-0 Medline

14. X. Wu, J. Wu, J. Huang, W. C. Powell, J. Zhang, R. J. Matusik, F. O. Sangiorgi, R. E. Maxson, H. M. Sucov, P. Roy-Burman, Generation of a prostate epithelial cell-specific Cre transgenic mouse model for tissue-specific gene ablation. *Mech. Dev.* **101**, 61–69 (2001). doi:10.1016/S0925-4773(00)00551-7 Medline

15. L. C. Trotman, M. Niki, Z. A. Dotan, J. A. Koutcher, A. Di Cristofano, A. Xiao, A. S. Khoo, P. Roy-Burman, N. M. Greenberg, T. Van Dyke, C. Cordon-Cardo, P. P. Pandolfi, Pten dose dictates cancer progression in the prostate. *PLOS Biol.* **1**, E59 (2003). doi:10.1371/journal.pbio.0000059 Medline

16. Z. Ding, C.-J. Wu, G. C. Chu, Y. Xiao, D. Ho, J. Zhang, S. R. Perry, E. S. Labrot, X. Wu, R. Lis, Y. Hoshida, D. Hiller, B. Hu, S. Jiang, H. Zheng, A. H. Stegh, K. L. Scott, S. Signoretti, N. Bardeesy, Y. A. Wang, D. E. Hill, T. R. Golub, M. J. Stampfer, W. H. Wong, M. Loda, L. Mucci, L. Chin, R. A. DePinho, SMAD4-dependent barrier constrains prostate cancer growth and metastatic progression. *Nature* **470**, 269–273 (2011). doi:10.1038/nature09677 Medline

17. Z. Chen, L. C. Trotman, D. Shaffer, H.-K. Lin, Z. A. Dotan, M. Niki, J. A. Koutcher, H. I. Scher, T. Ludwig, W. Gerald, C. Cordon-Cardo, P. P. Pandolfi, Crucial role of p53-dependent cellular senescence in suppression of Pten-deficient tumorigenesis. *Nature* **436**, 725–730 (2005). doi:10.1038/nature03918 Medline

18. Z. Zhou, A. Flesken-Nikitin, D. C. Corney, W. Wang, D. W. Goodrich, P. Roy-Burman, A. Y. Nikitin, Synergy of p53 and Rb deficiency in a conditional mouse model for metastatic prostate cancer. *Cancer Res.* **66**, 7889–7898 (2006). doi:10.1158/0008-5472.CAN-06-0486 Medline

19. L. A. Maddison, B. W. Sutherland, R. J. Barrios, N. M. Greenberg, Conditional deletion of Rb causes early stage prostate cancer. *Cancer Res.* **64**, 6018–6025 (2004). doi:10.1158/0008-5472.CAN-03-2509 Medline

20. M. D. Muzumdar, B. Tasic, K. Miyamichi, L. Li, L. Luo, A global double-fluorescent Cre reporter mouse. *Genesis* **45**, 593–605 (2007). doi:10.1002/dvg.20335 Medline

21. J. Livet, T. A. Weissman, H. Kang, R. W. Draft, J. Lu, R. A. Bennis, J. R. Sanes, J. W. Lichtman, Transgenic strategies for combinatorial expression of fluorescent proteins in the nervous system. *Nature* **450**, 56–62 (2007). doi:10.1038/nature06293 Medline

22. Z. Zhou, A. Flesken-Nikitin, A. Y. Nikitin, Prostate cancer associated with p53 and Rb deficiency arises from the stem/progenitor cell-enriched proximal region of prostatic ducts. *Cancer Res.* **67**, 5683–5690 (2007). doi:10.1158/0008-5472.CAN-07-0768 Medline

23. H. Beltran, D. S. Rickman, K. Park, S. S. Chae, A. Sboner, T. Y. MacDonald, Y. Wang, K. L. Sheikh, S. Terry, S. T. Tagawa, R. Dhir, J. B. Nelson, A. de la Taille, Y. Allory, M. B. Gerstein, S. Perner, K. J. Pienta, A. M. Chinnaiyan, Y. Wang, C. C. Collins, M. E. Gleave, F. Demichelis, D. M. Nanus, M. A. Rubin, Molecular characterization of neuroendocrine prostate cancer and identification of new drug targets. *Cancer Discov.* **1**, 487–495 (2011). doi:10.1158/2159-8290.CD-11-0130 Medline

24. M. S. Kareta, L. L. Gorges, S. Hafeez, B. A. Benayoun, S. Marro, A.-F. Zmoos, M. J. Cecchini, D. Spacek, L. F. Z. Batista, M. O'Brien, Y.-H. Ng, C. E. Ang, D. Vaka, S. E. Artandi, F. A. Dick, A. Brunet, J. Sage, M. Wernig, Inhibition of pluripotency networks by the Rb tumor suppressor restricts reprogramming and tumorigenesis. *Cell Stem Cell* **16**, 39–50 (2015). doi:10.1016/j.stem.2014.10.019 Medline

25. L. R. Bohrer, S. Chen, T. C. Hallstrom, H. Huang, Androgens suppress EZH2 expression via retinoblastoma (RB) and p130-dependent pathways: A potential mechanism of androgen-refractory progression of prostate cancer. *Endocrinology* **151**, 5136–5145 (2010). doi:10.1210/en.2010-0436 Medline

26. P. Mu, Z. Zhang, M. Benelli, W. R. Karthaus, E. Hoover, C.-C. Chen, J. Wongvipat, S.-Y. Ku, D. Gao, Z. Cao, N. Shah, E. J. Adams, W. Abida, P. A. Watson, D. Prandi, C.-H. Huang, E. de Stanchina, S. W. Lowe, L. Ellis, H. Beltran, M. A. Rubin, D. W. Goodrich, F. Demichelis, C. L. Sawyers, *SOX2* promotes lineage plasticity and antiandrogen resistance in *TP53* and *RB1* deficient prostate cancer. *Science* **355**, 84–88 (2017).

27. J. Li, C. Yen, D. Liaw, K. Podsypanina, S. Bose, S. I. Wang, J. Puc, C. Miliaresis, L. Rodgers, R. McCombie, S. H. Bigner, B. C. Giovanella, M. Ittmann, B. Tycko, H. Hibshoosh, M. H. Wigler, R. Parsons, PTEN, a putative protein tyrosine phosphatase gene mutated in human brain, breast, and prostate cancer. *Science* **275**, 1943–1947 (1997). doi:10.1126/science.275.5308.1943 Medline

28. A. P. Bracken, D. Pasini, M. Capra, E. Prosperini, E. Colli, K. Helin, EZH2 is downstream of the pRB-E2F pathway, essential for proliferation and amplified in cancer. *EMBO J.* **22**, 5323–5335 (2003). doi:10.1093/emboj/cdg542 Medline

29. H. Hong, K. Takahashi, T. Ichisaka, T. Aoi, O. Kanagawa, M. Nakagawa, K. Okita, S. Yamanaka, Suppression of induced pluripotent stem cell generation by the p53-p21 pathway. *Nature* **460**, 1132–1135 (2009). doi:10.1038/nature08235 Medline

30. H. Sun, Y. Wang, M. Chinnam, X. Zhang, S. W. Hayward, B. A. Foster, A. Y. Nikitin, M. Wills, D. W. Goodrich, E2f binding-deficient Rb1 protein suppresses prostate tumor progression in vivo. *Proc. Natl. Acad. Sci. U.S.A.* **108**, 704–709 (2011). doi:10.1073/pnas.1015027108 Medline